Magnetic flux profiles in $Bi_{1.2}Pb_{0.3}Sr_{1.5}Ca_2Cu_3O_y$ and $NdBa_2Cu_3O_{7-\delta}$ superconductors and a simulation by critical-state models

N. Hari Babu and T. Rajasekharan
Defence Metallurgical Research Laboratory, Hyderabad 500 058, India

V. Seshu Bai
School of Physics, University of Hyderabad, Hyderabad 500 046, India
(Received 25 February 1997; revised manuscript received 27 May 1997)

The features of the flux profiles recorded for the sintered and press-sintered $Bi_{1.2}Pb_{0.3}Sr_{1.5}Ca_2Cu_3O_y$ (BSCCO), and sintered and melt-textured $NdBa_2Cu_3O_{7-\delta}$ (NdBCO) superconducting samples with widely different microstructures are analyzed. From the slope of the flux profiles (at $H_{ac}\rightarrow 0$) recorded for various dc fields, the intergranular J_{ci} (H_{dc}) for the BSCCO samples is determined, whose field dependence is found to follow Kim's model. Using the fit parameters thus obtained, the flux profiles for different H_{dc} could be simulated very well including features like nonlinearity at low fields, the presence of a peak, and the oscillatory behavior. The flux profile of the sintered NdBCO recorded with zero H_{dc} could also be simulated well using Kim's critical-state model. An analysis of the intragranular flux profile determined from the measured profile at high fields suggests a wide distribution of H_g^*, (the full penetration field of the grain) and thereby of the J_{cg}. This result is in agreement with the broad transition observed in the ac susceptibility of this sample, attributed to the presence of $Nd_{1+x}Ba_{2-x}Cu_3O_{7-\delta}$ precipitates that modify the local J_{cg} values drastically. All the sintered specimen show nearly 45% of flux penetration (into the sample) at low enough fields ($H_{dc}<40$ Oe), while the flux entry into the melt-textured NdBCO is $<3\%$. At high dc fields (4–8 KOe) the profile exhibits two distinct slopes that are associated with a flux entry initially into the microcracks and then into the grains, from the microstructural considerations. [S0163-1829(97)06941-5]

INTRODUCTION

The granular nature of high-temperature superconductors (HTSC's) is well studied by ac-magnetic-susceptibility measurements[1–12] to assess the contributions from the intergrain and intragrain regions with widely differing critical current densities J_{ci} and J_{cg}, respectively, and are analyzed using critical-state models.[13–16] The nature and density of weak links associated with the coupling between the grains can drastically be modified by melt texturing the HTSC's as is evidenced from their microstructures. However, a clear correlation is yet to be established between the weak-link properties and the microstructures of HTSC's. In an attempt to contribute in this direction, magnetic flux profiles of $Bi_{1.2}Pb_{0.3}Sr_{1.5}Ca_2Cu_3O_y$ (BSCCO) and $NdBa_2Cu_3O_{7-\delta}$ (NdBCO) superconductors with widely different microstructures is taken up for a detailed study. Campbell[17] suggested a sensitive and versatile method that uses a phase-sensitive detector to measure the flux distribution and to determine model-independent J_c in type-II superconductors. This method can be used to assess the J_c of a material in a dc-field regime that is not accessible to transport methods.[18] Ni *et al.*[19] used this method to measure J_{ci} and J_{cg} for a sintered $YBa_2Cu_3O_{7-\delta}$ superconductor at 77 K, while Dang *et al.*[20] have determined J_{cg} and the pinning strength of $Bi_{1.7}Pb_{0.3}Sr_2Ca_2Cu_3O_y$. The pinning parameters like J_c, reversible penetration depth λ' of a pinned flux lattice, and the reversible displacement d, which is the distance flux can move before being unpinned have been determined from magnetic flux profile measurements by Küpfer *et al.*[21] and a comparison is made between low-T_c superconductors and $YBa_2Cu_3O_{7-\delta}$.

In the present study the magnetic flux profiles have been measured for the sintered and press-sintered BSCCO, sintered and melt-textured NdBCO. The features observed in the profiles are examined in the light of the corresponding microstructures and possible correlation of the results to the nature of weak links is proposed. The critical current densities are determined and their field dependence is analyzed in terms of critical-state models.

EXPERIMENT

A. Sample details

The four samples used in the present study are sintered $Bi_{1.2}Pb_{0.3}Sr_{1.5}Ca_2Cu_3O_y$ (sample A), press-sintered $Bi_{1.2}Pb_{0.3}Sr_{1.5}Ca_2Cu_3O_y$ (sample B), sintered $NdBa_2Cu_3O_{7-\delta}$ (sample C), and melt-textured $NdBa_2Cu_3O_{7-\delta}$ with 15 mol. % $Nd_4Ba_2Cu_2O_{10}$ (sample D).

Samples A and B were prepared from citrate precursors and the details of sample preparation, x-ray diffraction (XRD), and microstructural studies have been reported in Refs. 22 and 7. The zero resistivity temperatures are 106.4 and 105.9 K, respectively. The XRD results showed texturing along the c axis of the unit cell in the press-sintered sample. The scanning electron micrographs (SEM) of the fractured surface showed sample A to be highly porous, while the porosity was reduced on press sintering. The average size of the grains, which is $\sim 5\ \mu$m in sample A, gets reduced to $\sim 1\ \mu$m in sample B. The porosity is determined to be 50 and 15% for samples A and B, respectively.

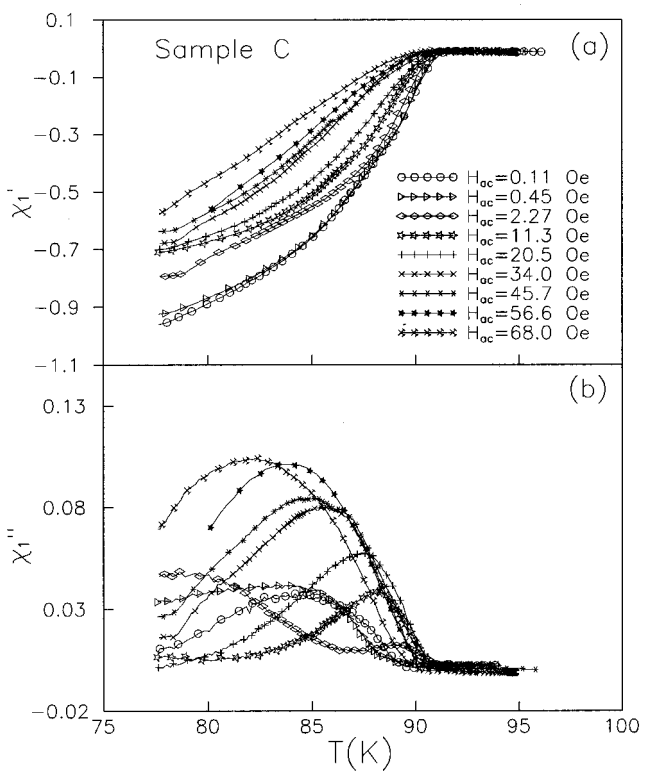

FIG. 1. Temperature dependence of the (a) real part (χ_1') and (b) imaginary part (χ_1'') of the fundamental susceptibility for sintered $NdBa_2Cu_3O_{7-\delta}$ (sample C) for different ac fields at 77 K.

Sample C is the sintered $NdBa_2Cu_3O_{7-\delta}$ (NdBCO). Presintered $NdBa_2Cu_3O_{7-\delta}$ powder was made into a pellet and held at 980 °C for 12 h in the reduced oxygen partial pressures to suppress the formation of solid solutions of type $Nd_{1+x}Ba_{2-x}Cu_3O_{7-\delta}$. Closely packed grains of size ~ 15 μm are seen in the SEM. Porosity is estimated to be $<5\%$. Zero resistivity temperature is 91 K. Temperature variation of χ_1' (real component of ac susceptibility) showed [Fig. 1(a)] a broad diamagnetic transition, indicative of a distribution of T_c's in the sample. In addition to the intergranular loss peak seen [Fig. 1(b)] in the temperature variation of χ_1'' at low ac fields, an intragranular loss peak appeared at higher fields which is also found to shift, unusually to low temperatures as the ac field is increased to a few tens of oersteads. This suggests that the grain J_c is also considerably field dependent. Even though the XRD has shown a nearly single phase formation, there seems to be solid solutions of $Nd_{1+x}Ba_{2-x}Cu_3O_{7-\delta}$ present at lower concentrations which would bring down the T_c of a region locally. This can cause a wide distribution of T_c resulting in the broad transition seen. The fact that solid solutions of $Nd_{1+x}Ba_{2-x}Cu_3O_{7-\delta}$ (Ref. 23) can have T_c's ranging from 92 to 25 K with x supports this picture.

Processing and the microstructural details of melt-textured sample D are given elsewhere.[24] The sample consists of domains of size 7–8 mm, without any liquid phase segregation at the boundaries. The domains are observed to contain Nd-123 platelets of average size 2.5 μm separated by cracks of average width 0.2 μm and fine uniformly distributed $Nd_4Ba_2Cu_2O_{10}$ (422) inclusions. Zero resistivity temperature is 92.5 K with the transition width of 0.9 K. Temperature variation of the ac susceptibility shows that the diamagnetic transition is very sharp confirming the suppression of solid solubility, and no traces of weak links.

B. Magnetic flux profile measurements

The magnetic flux profiles are measured using the ac inductive method, proposed by Campbell.[17] ac (33 Hz) and dc fields are applied along the length of the sample placed in one of the secondaries of a mutual inductance assembly. In general, ac field amplitudes are sufficiently small so that J_c is independent of the field over the amplitude of the ac signal. The in-phase signal (S) which is a measure of the magnetization at maximum $H_{\rm ac}$, is measured as a function of the amplitude of the ac field at 77 K for all the samples. This is repeated at various fixed dc fields. The flux penetration (p) into a sample of radius (R) can be calculated as a function of ac field amplitude at various constant dc fields using the equation

$$p = R - r = R\left(1 - \sqrt{\frac{-1}{K}\frac{dS}{dH_{\rm ac}}}\right), \tag{1}$$

where K is calibration constant which differs from that in Campbell's method. The above equation is derived to account for the present configuration where the resultant voltage from the two secondaries is adjusted to be nullified in the absence of a sample rather than with the sample in the Meissner state.

C. Calibration of the penetration depth

When the sample is in one of the secondary coils, the output of a pair of secondaries connected in opposition is given by[25,26]

$$\mu_o \alpha N V \omega (1-D)\frac{dM(\theta)}{d\theta},$$

where N is the number of turns per unit length of the secondary coil, V is the volume of the sample, ω is the angular frequency of the applied ac field, D is the demagnetization factor of the sample, α is the filling factor,[27] and $M(\theta)$ is the magnetization at a phase angle θ with respect to that of the ac field. The in-phase signal (S) measured by the lock-in amplifier in flat band mode is given by $S = KM$, where $K = 4\mu_o \alpha N V f (1-D)$ is the calibration factor which is a measure of the signal per gauss when the sample is in the Meissner state.

RESULTS AND DISCUSSION

A. Flux profiles

1. Profiles with $H_{dc}=0$

The magnetic flux profiles measured at 77 K in all the four samples with no external dc field are shown in Fig. 2. In the case of sintered BSCCO (sample A), the normalized penetration depth (p/R) increases nonlinearly with field and shows a peaklike structure at 8 Oe, which is the field (H_i^*) at which full penetration of flux takes place into the intergranular region. The penetration remains constant at p^* between 10 and 30 Oe, the lower critical field of the grains (H_{c1g}).

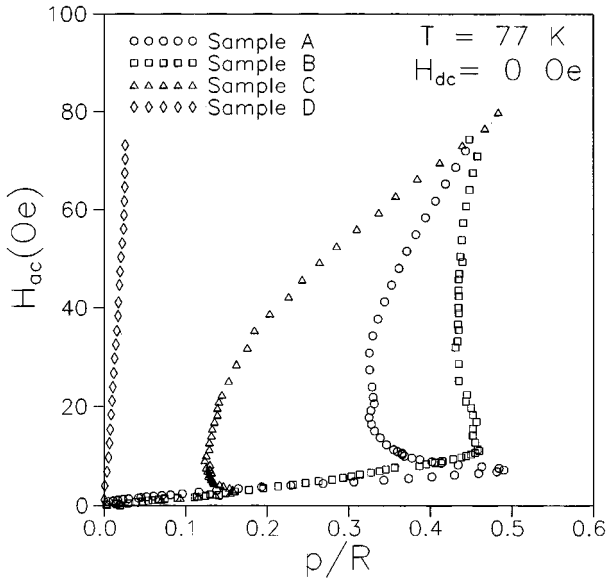

FIG. 2. Magnetic flux profiles (H_{ac} versus p/R) for sintered BSCCO (sample A), press-sintered BSCCO (sample B), sintered NdBCO (sample C), and melt-textured NdBCO (sample D) in the absence of dc field.

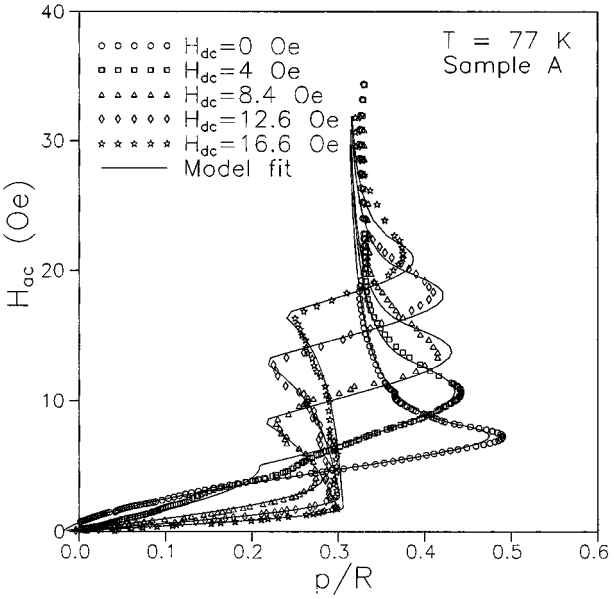

FIG. 3. Flux profiles in sintered $Bi_{1.2}Pb_{0.3}Sr_{1.5}Ca_2Cu_3O_y$ (sample A) at various dc fields and at 77 K. Solid lines are a simulation of Kim's critical-state model.

Above H_{c1g}, the flux starts penetrating into the grains in the form of Abrikosov vortices. This picture of step-wise flux penetration was visualized by Koblischka *et al.*[28] in granular $YBa_2Cu_3O_{7-\delta}$ using the high-resolution Faraday effect technique. For a granular sample, the effective p^*/R value is related to the grain fraction through $f_g=(1-p^*/R)^2$. In Fig. 2, from the vertical asymptotic line at $p^*/R=0.33$, f_g is estimated to be 0.45 and is quite comparable to the 50% porosity observed in the microstructure.

The flux profile in press-sintered BSCCO (sample B) is nearly linear at low fields, suggesting a weaker field dependence of J_c. The peaklike structure is less pronounced and the penetration remains constant up to the maximum ac field applied (80 Oe). Full penetration for intergranular region occurred at 11 Oe and the vertical asymptotic line at $p^*/R=0.41$, gives a value of 0.35 for f_g. Though the microstructure shows only 15% porosity (suggesting $f_g=0.85$), the measured f_g of 0.35 has its origin in an increase in the effective volume of flux penetration into the intergranular region which is a result of the smaller size ($\sim 1\,\mu$m) of the grains on press sintering, compared to sample A with grains of 5 μm. The enhancement in the apparent lower critical field H_{c1g} value (>80 Oe) on press sintering is probably due to the surface barrier effect discussed by Bean and Livingston.[29]

In the case of sintered NdBCO (sample C), magnetic flux has penetrated up to the center of the sample through the intergranular region for 4 Oe and the flux profile is nonlinear. The value of f_g is 0.8 as estimated from the observed $p^*/R=0.11$. This is consistent with the volume fraction of the grain region estimated from the optical micrographs, which showed that 85% of the sample is occupied by the grains of nearly equal size ($\sim 15\,\mu$m) separated by relatively smaller interface regions.

Melt processing has enormously reduced the rate of flux penetration into the sample with respect to the field amplitude. Moreover, there are no two distinct slopes as in the case of the three sintered samples indicating the absence of predominant granularity.

2. Profiles with $H_{dc}\neq 0$

The intergranular properties have been studied by superimposing an ac field on various fixed dc fields. Figures 3 and 4 show the effect of applying different dc fields on the flux profiles in the sintered and press-sintered BSCCO. For the sintered one (sample A) at low ac fields, the flux profiles are linear with their slope reducing as the dc field is increased. When H_{ac} is comparable to H_{dc}, an oscillatory behavior is

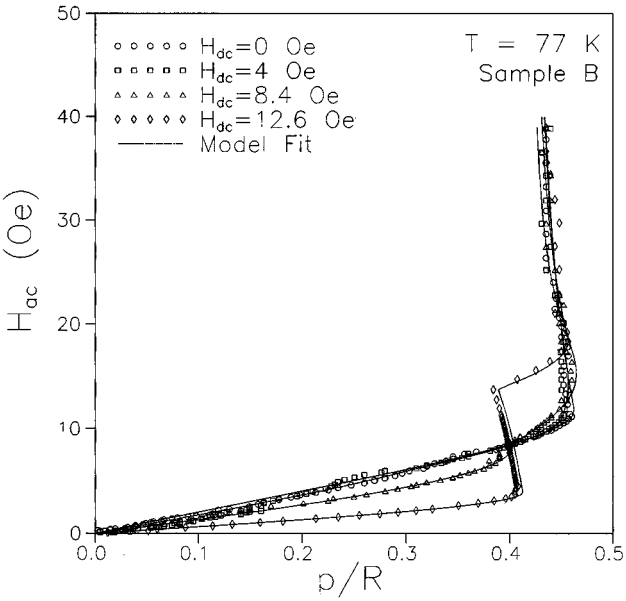

FIG. 4. Flux profiles in press-sintered $Bi_{1.2}Pb_{0.3}Sr_{1.5}Ca_2Cu_3O_y$ (sample B) at various dc fields and at 77 K. Solid lines are a simulation of Kim's critical-state model.

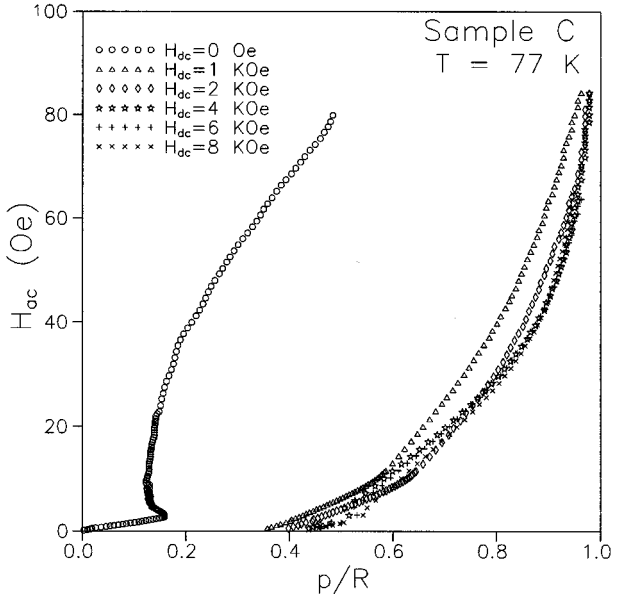

FIG. 5. Flux profiles in sintered $NdBa_2Cu_3O_{7-\delta}$ (sample C) at various dc fields and at 77 K.

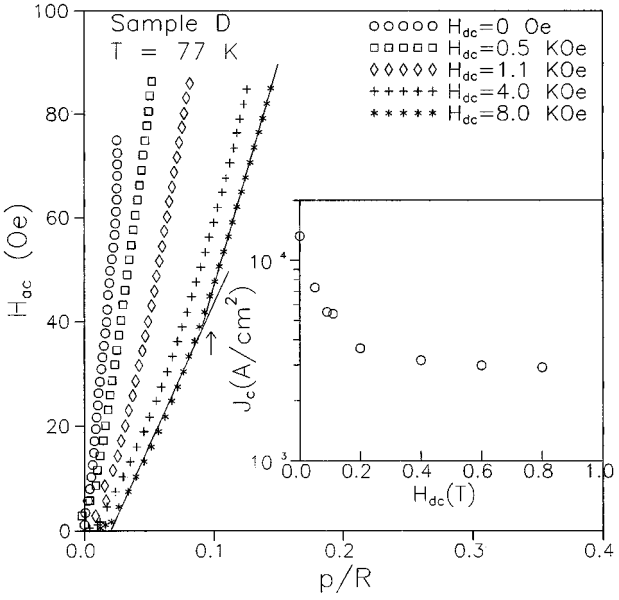

FIG. 6. Flux profiles in melt-textured NdBCO (sample D) at various dc fields and at 77 K. Arrow mark shows the crossover of two distinct slopes. The inset shows the field dependence of critical current density.

seen in the flux profiles. The press-sintered one (sample B) also exhibits a similar behavior but the amplitude of oscillation is less.

Figure 5 shows the magnetic flux penetration into the sintered NdBCO (sample C) in the presence of different dc-field strengths. Normalized penetration (p/R) has reached a value of 1 for $H_{dc}=1$ KOe indicating the flux penetration to be complete into the entire sample including the grains. By increasing the dc field further, the slope of the flux profiles has reduced, indicating a strong field dependence of J_{cg} of the grains, which reflected as a shift in the intragranular loss peak in $\chi_1''(T)$ curves with an increase in the ac-field amplitude.

Flux penetration into the melt-processed NdBCO with 422 inclusions (sample D) is shown in Fig. 6. SEM of the sample showed that cracks with an average size of 0.2 μm separate the platelets (grains) of size 2.5 μm and are uniform and not continuous. Since the density of cracks and the pinning centers (422 particles) are rather uniform as seen from the microstructure, the flux penetration is expected to be linear and pass through the origin, based on Bean's[13] critical-state model. But the measured flux profiles exhibit a shift along the p/R axis which represents the ''reversible penetration depth.'' [17,21] A detailed work on the variation of this parameter in melt-textured samples with varying concentration of pinning centers (422 inclusions) and the nature of microcracks will be reported elsewhere. At large dc fields, p/R has reached a value of 0.15 at 8 KOe field and the profile is found to have two distinct slopes at high dc fields. The first slope can be associated with a J_c corresponding to the flux penetration into the specimen through the cracks, while the second is associated with the J_c of the grains themselves which is much larger as indicated by the smaller extent of penetration at large ac fields. This picture is supported by the high-resolution Faraday measurements of Schuster *et al.*[30] on melt-processed $YBa_2Cu_3O_{7-\delta}$, which indicate that the flux penetrates [Figs. 2(c) and 2(d) in Ref. 30] the sample preferentially along the cracks and then into the matrix.

B. Determination of critical current density (J_c)

The slope of the flux profiles near the origin in the linear regime is directly related to the critical current density J_c of that region and is model independent. Figure 7 shows the field dependence of J_{ci} for samples A and B calculated using[20]

$$J_{ci}=\frac{dH_{ac}}{d(p/R)}\,\frac{1-f_g}{R}. \tag{2}$$

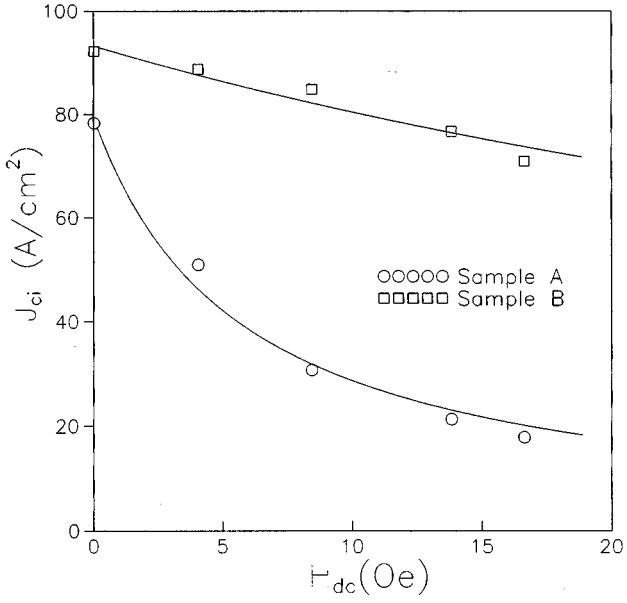

FIG. 7. Field variation of intergranular J_{ci} determined from the linear regime of flux profiles for samples A and B. Solid line is a fit to the equation $J_{ci}=K/(H_{dc}+H_0)$.

J_{ci} determined for the sintered BSCCO is smaller and shows greater field dependence than for the press-sintered BSCCO and is found to vary as $J_{ci}(H_{dc})=K/(H_{dc}+H_0)$ for both the above samples with fit parameters $K=3.58\times10^8$ A^2/m^3, $H_0=450$ A/m for sample A and $K=4.67\times10^9$ A^2/m^3, $H_0=5010$ A/m for sample B. Simulation of the measured profiles using the critical-state model is discussed in the next section.

The bulk J_c values of the melt-textured NdBCO (sample D) are calculated for different dc fields from the flux profiles using the formula $J_c=[dH_{ac}/d(p/R)]/R$, at low ac fields, and they vary as shown in the inset of Fig. 6 with H_{dc}.

For sample C, J_{ci},J_{cg} are arrived at from a theoretical simulation of the measured data as described below, instead of recording a large number of profiles at different H_{dc}.

C. Theoretical model calculations

We have presented here the calculation of the flux profiles of an infinitely long cylinder with radius R of type-II superconductors exposed to an external field $H=H_{dc}+H_{ac}\cos(\omega t)$ along the axis of the cylinder, based on Kim's critical-state model. We denote the maximum and minimum values of H by $H_A=H_{dc}+H_{ac}$ and $H_B=H_{dc}-H_{ac}$. The average flux density $B(H)$ in the sample can be calculated as

$$B(H)=\frac{2}{R^2}\int_0^R xB_i(x)dx,$$

where $B_i(x)$ is local flux density. The penetration depth

$$p=R\left(1-\sqrt{1-\frac{\mu_c d[B(H_A)-B(H_B)]}{2\mu_0 dH_{ac}}}\right)$$

is calculated for the three cases namely for $0<H_A<H_p$, $H^*\leqslant H_A$, and $H_p\leqslant H_A\leqslant H^*$, where H_p is the full penetration field and H^* is the field at which reverse supercurrent penetrates to the center of the specimen before H is cycled back to zero. When H_{dc} has a nonzero value, each of these cases is further classified into several different cases, depending on the magnitude of H_B. The detailed calculations for $B(H)$ in all possible cases are given in Ref. 31. By taking the same fit parameters given in the previous section, p/R is calculated as a function of H_{ac} for samples A and B. Using these, the entire region of flux profiles including the features like the nonlinearity, the peak, and the oscillatory behavior could be very well simulated as shown in Figs. 3 and 4 as solid lines. The larger J_{ci}, the less pronounced peak, and the near linearity of the flux profiles for sample B indicate that the coupling between the grains has been strengthened compared to that in the sintered sample. The oscillatory behavior seen when H_{dc} is comparable to H_{ac} is due to the effective magnetic field becoming zero at some local regions inside the sample where the screening could be better and effectively J_c is higher than in zero H_{dc}.

For the sintered NdBCO (sample C), the flux profiles shown in Fig. 5 are nonlinear in the absence of a dc field and exhibit a complete penetration of flux even through the grains at $H_{dc}=1$ KOe as indicated by $p/R=1$. The solid line in Fig. 8 shows that the profile at $H_{dc}=0$ fits quite well to Kim's critical-state model with $K=3.9\times10^7$ A^2/m^3, and

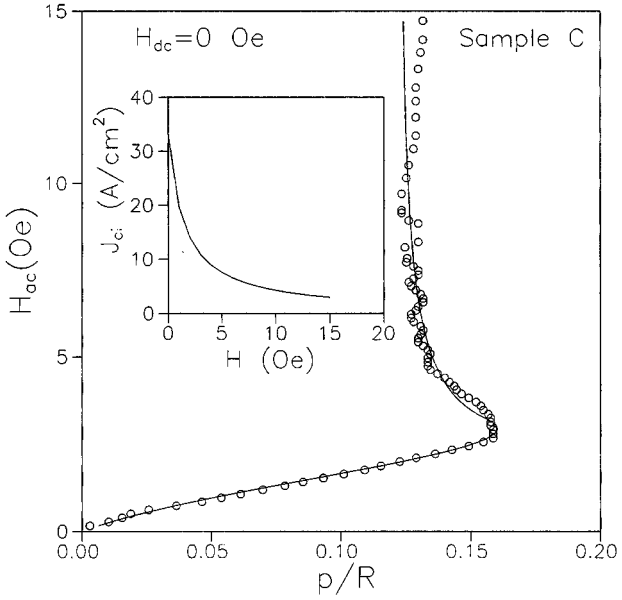

FIG. 8. Simulation of the measured flux profile in the absence of dc field for sintered NdBCO (sample C) of Kim's critical-state model. The inset shows the field variation of J_{ci} calculated from the fit parameters of K and H_0.

$H_0=118$ A/m, and this comes from the intergranular region. The $J_{ci}(H_{dc})$ calculated with the above fit parameters is shown as an inset in Fig. 8.

Since the slope of the profiles at large dc fields reduces with the field, it is necessary to invoke a field dependence for J_{cg} as well for a complete theoretical analysis. For this purpose, the flux profile into the grains is extracted from the global flux profile using $p_g/R_g=1-(1-p/R)/(1-p^*/R)$, where p_g is the extent of penetration into the grain and is shown in Fig. 9. The dashed line is a fit to Kim's critical-state model taking the grain radius (R_g) to be 7.5 μm and can be seen to deviate considerably from the measured profile. Considering this deviation to be due to a local distribution in J_{cg} due to the presence of $Nd_{1+x}Ba_{2-x}Cu_3O_{7-\delta}$ precipitates in the grains [that were also responsible for a broader $\chi_1'(T)$ transition, Fig. 1(a)] a Gaussian distribution described by the function $f(J_{cg})=A\exp(-(J_{cg}-J_{cj0})^2/2\Delta^2)$ is invoked. (Here A is a normalization constant, J_{cg0} is the mode of the distribution in the critical current density (J_{cg}) that represents the average value, and Δ is the half width at half maximum). The grain profile thus calculated using Kim's critical-state model is shown as a solid line in Fig. 9. For $J_{cg0}=1.85\times10^5$ A/cm^2 and $\Delta=1.6\times10^5$ A/cm^2, the agreement of the theoretical curve with the measured profile can be seen to be very good. The inset in Fig. 9 shows the expected field dependence of the average intragranular J_{cg0} calculated using the fit parameters $K=5.1\times10^{13}$ A^2/m^3 and $H_0=27\,760$ A/m for the intragranular region.

CONCLUSIONS

The flux profiles (H_{ac} versus p/R) in sintered BSCCO and NdBCO samples exhibit a nonlinear curve at very low fields followed by a peaklike structure at full penetration field H_i^*

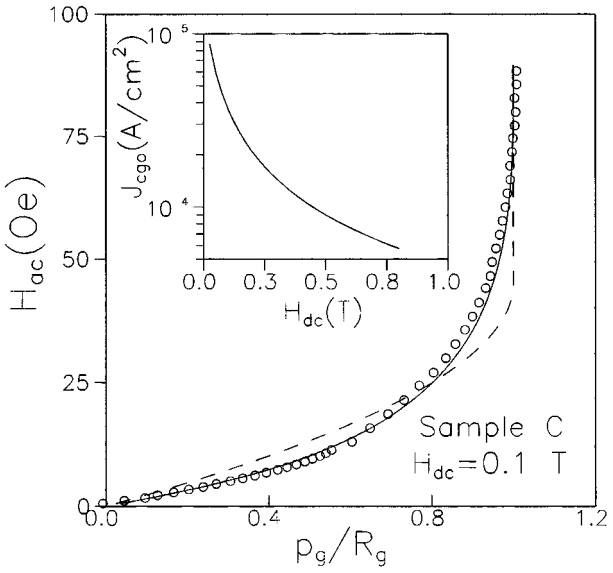

FIG. 9. The profile into the grains as extracted from the measured global flux profile. The solid line is a fit to Kim's critical-state model after incorporating a Gaussian distribution in J_{cg}. Deviation from the experimental data can be seen (dashed line) when a single valued J_{cg} is considered. The inset shows the field variation of J_{cgo}.

into the intergrain region. At $H_{ac}>H_i^*$ the penetration remains constant up to the lower critical field of the grains above which the flux profile into the grains is obtained. The H_i^* and J_{ci} are found to be enhanced for BSCCO sample on press sintering. This has a correlation to the reduction in porosity and the resultant strengthening of the coupling between the grains. The enhancement in the apparent lower critical field H_{c1g} value on press sintering is probably due to the existence of a surface barrier to the penetration of magnetic flux. $J_{ci}(J_{dc})$ has been determined from the slope of the flux profile in the linear regime and is found to vary as $K/(H_{dc}+H_0)$. Using the fit parameters K and H_0 of Kim's critical-state model, all the features of flux profiles observed experimentally could be very well simulated.

The sintered NdBCO sample with a broad susceptibility transition due to $Nd_{1+x}Ba_{2-x}Cu_3O_{7-\delta}$ precipitates is found to show complete penetration into the intergrain region at $H_{ac}=4$ Oe with $H_{dc}=0$ Oe and into even the grains at $H_{ac}\sim 50$ Oe with $H_{dc}=1$ KOe. The grain fraction f_g calculated from the flux profile is consistent with the estimated grain fraction from optical micrographs. Both the intergranular profile recorded at $H_{dc}=0$ and the grain flux profile derived from the global profile recorded at high fields could be simulated well using Kim's critical-state model. However, for the latter fit, it was necessary to invoke a wide distribution in the grain critical current density J_{cg}, possibly arising locally due to the low-T_c phase of type $Nd_{1+x}Ba_{2-x}Cu_3O_{7-\delta}$ (which is also evidenced by the broad transition in the temperature variation of the ac susceptibility). The flux penetration into the melt-processed samples is much slower compared to the sintered samples due to stronger coupling between the domains. p/R is less than 0.03 at low H_{dc}, while it is 0.15 even at the 8 KOe field. At high fields ($H_{dc}=4-8$ KOe) the flux profiles were found to exhibit two different slopes. From the microstructural considerations and the high-resolution Faraday results of Schuster *et al.*, these slopes are attributed to be representing the flux entry initially into the microcracks between the grains and then into the grains themselves.

ACKNOWLEDGMENTS

N.H.B. is grateful to the CSIR for financial support and V.S.B. thanks UGC for the research project.

[1] M. Nikolo and R. B. Goldfarb, Phys. Rev. B **39**, 6615 (1988).
[2] D. X. Chen, J. Nogues, and K. V. Rao, Cryogenics **29**, 800 (1989).
[3] D. X. Chen, A. Sanchez, T. Puig, L. M. Martinez, and J. S. Muñoz, Physica C **168**, 652 (1990).
[4] T. Ishida and R. B. Goldfarb, Phys. Rev. B **41**, 8937 (1990).
[5] L. Ji, R. H. Sohn, G. C. Spalding, C. J. Lobb, and M. Tinkham, Phys. Rev. B **40**, 10 936 (1989).
[6] Y. Kim, Q. Harry Lam, and C. D. Jefferies, Phys. Rev. B **43**, 11 404 (1991).
[7] S. Ravi and V. Seshu Bai, Phys. Rev. B **49**, 13 082 (1994).
[8] S. Ravi and V. Seshu Bai, Physica C **230**, 51 (1994).
[9] O. F. Schilling, K. Aihaora, A. Soeta, T. Kamo, and S. Matsuda, Phys. Rev. B **47**, 8096 (1993).
[10] D. Berling, E. V. Antipov, J. J. Capponi, M. F. Gorius, B. Loegel, A. Mehdaoui, and J. L. Tholence, Physica C **225**, 212 (1994).
[11] X. C. Jin, Y. Y. Xue, Z. J. Huang, J. Bechtold, P. H. Hor, and C. W. Chu, Phys. Rev. B **47**, 6082 (1993).
[12] M. G. Karkut, M. Slaski, L. K. Sagdahl, and K. Fossheim, Physica C **215**, 19 (1993).
[13] C. P. Bean, Phys. Rev. Lett. **8**, 250 (1962); Rev. Mod. Phys. **36**, 31 (1964).
[14] Y. B. Kim, C. F. Hempstead, and A. R. Strnad, Phys. Rev. Lett. **9**, 306 (1962).
[15] Y. B. Kim, C. F. Hempstead, and A. R. Strnad, Phys. Rev. **129**, 528 (1963).
[16] G. Ravi Kumar and P. Chaddah, Phys. Rev. B **39**, 4704 (1989).
[17] A. M. Campbell, J. Phys. C **2**, 1492 (1969).
[18] A. M. Campbell and F. J. Blunt, Physica C **172**, 253 (1990).
[19] B. Ni, T. Munakata, T. Matsushita, M. Iwakuma, K. Funki, M. Takeo, and K. Yamafuji, Jpn. J. Appl. Phys., Part 1 **27**, 1658 (1988).
[20] A. Dang, P. Godelaine, Ph. Vanderbemden, R. Cloots, and M. Ausloos, J. Appl. Phys. **77**, 3560 (1995).
[21] H. Küpfer, A. A. Zhukov, R. Kresse, R. Meier-Hirmer, W. Jahn, T. Wolf, T. Matsushita, K. Kimura, and K. Salama, Phys. Rev. B **52**, 7689 (1995).
[22] V. Seshu Bai, S. Ravi, T. Rajasekharan, and R. Gopalan, J. Appl. Phys. **70**, 4378 (1991).
[23] T. B. Lindemer, E. D. Specht, P. M. Martin, and M. L. Flitcroft, Physica C **255**, 65 (1995).
[24] N. Hari Babu and T. Rajasekharan (unpublished).
[25] F. Gömöry, Rev. Sci. Instrum. **62**, 2019 (1991).
[26] G. E. Gough, M. S. Colclough, D. A. O'Conner, F. Wellhofer, N.

McN. Alford, and T. W. Button, Cryogenics **31**, 119 (1991).
[27] M. Couach and A. F. Khoder, in *Magnetic Susceptibility of Superconductors and Other Spin Systems*, edited by R. A. Hein *et al.* (Plenum, New York, 1992).
[28] M. R. Koblischka, Th. Schuster, and H. Kronmüller, Physica C **219**, 205 (1994).
[29] C. P. Bean and J. D. Livingston, Phys. Rev. Lett. **12**, 14 (1964).
[30] Th. Schuster, M. R. Koblischka, H. Kuhn, M. Glücker, B. Ludescher, and H. Kronmüller, J. Appl. Phys. **74**, 3307 (1993).
[31] K. Yamamoto, H. Mazaki, and H. Yasuoka, Phys. Rev. B **47**, 915 (1993).